Fusion Engineering and Design 231 (2026) 115966

Contents lists available at ScienceDirect

Fusion Engineering and Design

journal homepage: www.elsevier.com/locate/fusengdes

Segregated and block-coupled approaches for electric potential coupling in multi-region magnetohydrodynamic flows within fusion liquid metal breeding blankets☆

B. Lyu *, L. Bühler, C. Mistrangelo

Karlsruhe Institute of Technology (KIT), P.O. Box 3640, 76021 Karlsruhe, Germany

ARTICLE INFO

Keywords:
Magnetohydrodynamics (MHD)
ITER WCLL blankets
Numerical modeling
Electromagnetic coupling
Solver development
Validation

ABSTRACT

Liquid metal breeding blankets in fusion reactors operate under strong magnetic fields, which results in the occurrence of complex magnetohydrodynamic (MHD) effects driven by electric currents that couple fluid and solid regions. Accurate modeling of this electromagnetic coupling is essential for reliable prediction of MHD flows in fusion blankets. This work compares two numerical strategies for electric potential coupling in multi-region MHD flows: a block-coupled and a segregated approach. The block-coupled method solves the governing equations in all regions simultaneously, providing strong interface coupling and rapid convergence, but requires strict mesh conformity at fluid–solid interfaces, which is difficult to achieve in complex geometries using automatic meshing tools. A segregated multi-region solver that solves the governing equations sequentially, tolerates nonconforming meshes through iterative interface coupling. The segregated approach is validated and applied to simulations of liquid metal flow in a mock-up of a water-cooled lithium lead test blanket module for ITER. Numerical results show good agreement with experimental observations and confirm a strongly non-uniform liquid metal flow distribution among the breeder units. The study highlights the respective strengths and limitations of both approaches and provides guidance for selecting appropriate electric potential coupling strategies in high fidelity simulations of blanket systems for ITER and DEMO.

1. Introduction

Tritium self-sufficiency is an indispensable operational criterion for future fusion power reactors, as it enables a sustainable fuel cycle in which the reactor compensates for its tritium consumption through in-situ breeding, thereby overcoming the global scarcity of tritium and ensuring long term fusion power plant viability. The water-cooled lithium lead (WCLL) breeding blanket is one of the concepts under development and foreseen as test blanket module (TBM) for ITER. The current design [1] is shown in Fig. 1. The liquid metal PbLi flows in two columns being distributed in 2×8 Breeding Units (BU) through the feeding poloidal manifolds before it reaches the draining manifolds. The poloidal–radial and toroidal–radial stiffening plates ensure compliance with structural requirements, while the baffle plates guide the flow of liquid metal inside each BU.

In the flow of the electrically conducting PbLi through the plasma-confining intense magnetic field, electric currents are induced that generate electromagnetic Lorentz forces acting on the flow. Electromagnetic forces are responsible for large additional magnetohydrodynamic (MHD) pressure drop. Along its flow path, the liquid breeder changes direction several times from toroidal to poloidal and radial directions. Previous studies show that changes in flow paths may lead to significant pressure drop and pronounced distortions of the velocity distribution compared to hydrodynamic conditions, in particular when multiple parallel ducts are electrically coupled by the solid structure, such as stiffening plates or baffle walls [3–5]. Consequently, electromagnetic coupling at the fluid–solid interface and between neighboring fluid domains has to be taken into account for accurate modeling of MHD flows in fusion blankets.

These MHD phenomena can lead to non-uniform flow distribution and uneven residence time of PbLi within the BUs arranged in a column. This affects tritium transport and leads to localized regions with elevated tritium concentration, while other regions become depleted. Over time, these effects may degrade the tritium breeding performance and raise safety concerns due to localized accumulation of tritium. In addition, tritium may diffuse into unintended regions, such as the coolant water or structural materials, thereby reducing the overall tritium recovery efficiency. Consequently, the PbLi flow distribution must

☆ This article is part of a Special issue entitled: 'ISFNT-16' published in Fusion Engineering and Design.

* Corresponding author.
E-mail address: biao.lyu@kit.edu (B. Lyu).

https://doi.org/10.1016/j.fusengdes.2026.115966
Received 30 January 2026; Received in revised form 13 July 2026; Accepted 20 July 2026
Available online 31 July 2026

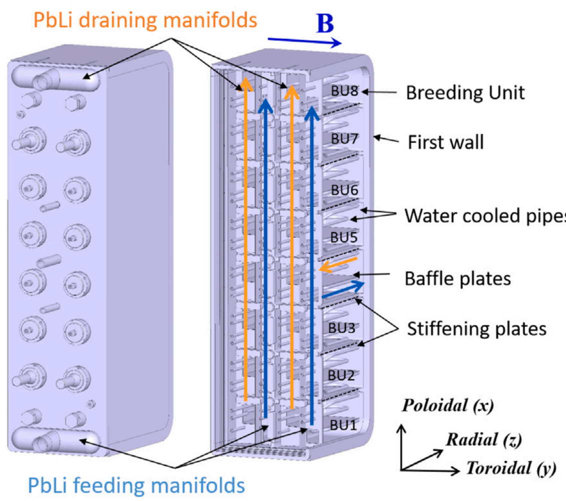

Fig. 1. CAD design of WCLL TBM as provided by CEA. [2].

be carefully analyzed and optimized during blanket design. A previous experimental campaign investigated the MHD flow in a WCLL TBM mock-up [6]. While the experimental data already reveals uneven flow distribution in BUs by pressure and potential measurements [7], only numerical simulations may provide insight into internal flow details and support design revisions.

Moreover, as breeding blanket concepts evolve, thermo-mechanical and thermo-hydraulic simulations must be repeatedly performed to assess the impact of modifications. A key challenge in such analyses is the accurate modeling of electromagnetic coupling at fluid–solid interfaces in multi-region MHD flows. To address this challenge, the present study develops and validates efficient numerical algorithms that enable faster and more robust simulations throughout the breeding blanket design cycle.

2. Numerical approaches for electric potential coupling in multi-region MHD flows

MHD flows are governed by the interactions of fluid dynamics and electromagnetism. When describing MHD flows mathematically, the following assumptions are made: the fluid is incompressible, displacement currents are neglected due to low frequency conditions, and the inductionless approximation is applied, assuming that the applied magnetic field is unaffected by the flow when the magnetic Reynolds number is small. The electromagnetic behavior in fluid and solid is governed by Ohm's law and charge conservation, which lead to a Poisson equation for the electric potential. The governing equations are summarized in Table 1, where $\mathbf{v}$, p, $\mathbf{j}$, $\mathbf{B}$, and ϕ represent velocity, pressure, electric current density, magnetic flux density, and electrical potential, respectively. The relevant material properties include the specific electric conductivity σ, kinematic viscosity ν, and mass density ρ. Subscript S indicates the parameter of the solid. The dimensionless parameters characterizing the flow are, the Hartmann number, the interaction parameter and the wall conductance parameter

$$Ha = B_0 L\sqrt{\frac{\sigma}{\rho\nu}},\ \ N = \frac{\sigma L B_0^2}{\rho u_0},\ c = \frac{\sigma_S t_w}{\sigma L}.$$

Here, B_0 denotes the magnitude of the applied magnetic field, while u_0 and L are the mean velocity and length scale. The square of the Hartmann number indicates the ratio of electromagnetic to viscous forces, whereas the interaction parameter expresses the ratio of electromagnetic to inertial forces. The electrical conductance of the wall with thickness t_w and conductivity σ_S compared to that of the fluid is characterized by the wall conductance parameter c.

Table 1
MHD equations for fluid and solid regions.

Fluid	Momentum conservation $\rho\left(\frac{\partial\mathbf{v}}{\partial t} + (\mathbf{v}\cdot\nabla)\,\mathbf{v}\right) = -\nabla p + \rho\nu\nabla^2\mathbf{v} + \mathbf{j}\times\mathbf{B}$
	Mass conservation $\nabla\cdot\mathbf{v} = 0$
	Ohm's law & charge conservation $\mathbf{j} = \sigma(-\nabla\boldsymbol{\phi} + \mathbf{v}\times\mathbf{B});\ \ \nabla\cdot\mathbf{j} = 0$
	Poisson equation for electric potential $\nabla^2\phi = \nabla\cdot(\mathbf{v}\times\mathbf{B})$
Solid	Ohm's law & charge conservation $\mathbf{j}_S = -\sigma_S\nabla\boldsymbol{\phi}_S;\ \ \nabla\cdot\mathbf{j}_S = 0$
	Poisson equation for electric potential $\nabla^2\phi_S = 0$

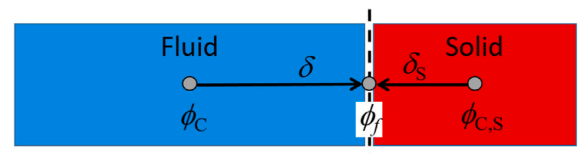

Fig. 2. Conditions at the fluid-wall interface.

Since electric potential and currents exist in both the fluid and solid domains, appropriate conditions must apply at their interface. Here the continuity of electric potential and wall normal current is assumed

$$\phi = \phi_S,\ \sigma\frac{\partial\phi}{\partial n} = -\sigma_S\frac{\partial\phi_S}{\partial n}\,, \tag{1}$$

where n is the normal direction that points outward of the respective domains. The interface between a fluid and a solid cell is shown in Fig. 2. Combining Eqs. (1) and approximating the wall normal derivatives by finite differences between face and cell-center values, ϕ_f and ϕ_C, for the fluid $(\phi_f - \phi_C)/\delta$ and for the solid, $(\phi_f - \phi_{S,C})/\delta_S$ we find a consistent interpolation

$$\phi_f = \omega\,\phi_{S,C} + (1-\omega)\,\phi_C, \tag{2}$$

where the abbreviation

$$\omega = \left(1 + \frac{\delta_S}{\delta}\frac{\sigma}{\sigma_S}\right)^{-1} \tag{3}$$

denotes a weighting factor that takes into account fluid and solid conductivity and distances between cell centers and the interface. For well conducting walls ($\sigma_S/\sigma \gg 1$), $\omega \to 1$, the interface potential reduces to $\phi_f = \phi_{S,C}$, a fixed value boundary condition. Conversely, for poor conducting walls ($\sigma_S/\sigma \to 0$), $\omega \to 0$, we find $\phi_f = \phi_C$, which corresponds to a zero gradient condition for the fluid. The weighting factor ω thus describes the strength of the numerical coupling between the fluid and solid regions.

The employed numerical solver is based on finite volume techniques implemented in the frame of the open source code OpenFOAM using a cell-centered finite volume method for discretization of the equations. Crucial for the solution for strong magnetic fields is a current conservative formulation of discretized equations for electric potential in fluid and solid domains and at their interfaces. Applying the divergence theorem to the potential equations for fluid and solid and integrating over the finite volumes bounded by their respective faces f with face area vector $\mathbf{S}_f$ we find the discrete representations

$$\sum_{f=1}^{n_f}(\nabla\phi)_f\cdot\mathbf{S}_f = \sum_{f=1}^{n_f}(\mathbf{v}\times\mathbf{B})_f\cdot\mathbf{S}_f, \tag{4}$$

$$\sum_{f=1}^{n_f}(\nabla\phi_S)_f\cdot\mathbf{S}_f = 0,. \tag{5}$$

where $(\nabla\phi)_f$ and $(\mathbf{v}\times\mathbf{B})_f$ denote the gradient of electric potential and flow-induced electric field interpolated to the respective face centroid f. Eqs. (4) and (5) lead to linear systems of equations for fluid and solid domains.

The treatment of variables at an interface between two dissimilar materials such as fluid and solid requires special attention. To clarify this, we consider as an example a fluid–solid interface f between two cells as shown in Fig. 2. Substituting the interpolation of the interface potential ϕ_f in Eq. (2), the potential gradients become

$$(\nabla\phi)_f = \frac{\phi_\mathrm{C}-\phi_f}{\delta} = \omega\frac{\phi_\mathrm{C}-\phi_\mathrm{S,C}}{\delta}\,, \tag{6}$$

$$\left(\nabla\phi_\mathrm{S}\right)_f = \frac{\phi_\mathrm{S,C}-\phi_f}{\delta_\mathrm{S}} = (1-\omega)\frac{\phi_\mathrm{S,C}-\phi_\mathrm{C}}{\delta_\mathrm{S}}\,. \tag{7}$$

Two numerical approaches are commonly employed for implementing Eqs. (6) and (7) across multi-region interfaces, i.e. the block-coupled and the segregated methods.

2.1. Block-coupled approach

The block-coupled MHD solver developed at KIT [8] in OpenFOAM-extend [9] couples the electrical equations for fluid and solid regions at the matrix level. In this approach, the potential Poisson equations for the electric potential across the entire computational domain are solved simultaneously. OpenFOAM-extend provides the `BlockLduMatrix` class to handle block matrices in a fully general and templated framework, enabling monolithic coupling across multiple regions. Originally developed by Jasak [10], it offers the flexibility required to assemble and solve multi-field systems. This feature allows the formulation of a joint coefficient matrix for the electric potential for fluid and solid domains representing the interdependence of Φ as block sub-matrices:

$$\begin{bmatrix}\mathbf{A}_\mathrm{FF} & \mathbf{A}_\mathrm{FS}\\ \mathbf{B}_\mathrm{SF} & \mathbf{B}_\mathrm{SS}\end{bmatrix}\begin{bmatrix}\Phi_\mathrm{C}\\ \Phi_\mathrm{S,C}\end{bmatrix} = \begin{bmatrix}\mathbf{a}\\ \mathbf{b}\end{bmatrix}. \tag{8}$$

$\mathbf{A}_\mathbf{FF}$ and $\mathbf{B}_\mathbf{SS}$ contain the coefficients linking the fluid and solid regions, respectively, to themselves, while $\mathbf{A}_\mathbf{FS}, \mathbf{B}_\mathbf{SF}$ represent the coupling terms between the fluid and solid domains. The fluid–solid interfaces are coupled and assembled into the sub-matrices $\mathbf{A}_\mathbf{FS}$ and $\mathbf{B}_\mathbf{SF}$, which enable information exchange between the interfaces and is facilitated by a specialized `regionCoupling` condition.

The electric potential for fluid and solid is stored in a single global solution vector and solved monolithically using a block coupled solver. Interface continuity is inherently enforced through the coupled matrix assembly, in contrast to the segregated approach where interface boundary conditions must be prescribed explicitly.

By embedding the coupling terms into a single global system matrix, inter-region interactions are resolved within each linear solution, which significantly improves convergence for strongly coupled problems as it avoids the iterative exchange of interface values. The approach enables direct access to multi-equation solution strategies through `BlockLduMatrix` or `coupledFvMatrix`, while remaining compatible with standard linear solvers, parallel execution, as well as multi-region utilities such as `splitMesh`.

One significant drawback is the substantially higher memory demand. In addition, the tight integration of equations reduces modularity, meaning that modifications to the physical model in one region may require corresponding structural changes to the entire block system. Moreover, the block-coupled approach requires strict mesh conformity at interfaces, which is not always guaranteed by automatic meshing tools when applied to complex geometries as encountered in fusion engineering applications. Although strict conformity could be enforced through manual block-structured meshing, this substantially increases preprocessing efforts and severely limits geometric flexibility.

Further constraints arise from decomposition for parallelization, since fluid and solid cells with common interfaces must be contained within same processor partitions, limiting domain decomposition strategies and often degrading load balancing. Finally, the implementation in OpenFOAM-extend, while very powerful, lacks many of the more advanced features and workflow capabilities available in the main OpenFOAM branch, which can restrict its applicability in modern simulation environments.

In practice, the block-coupled approach makes it difficult to simulate multi-region MHD flow in the complex WCLL TBM geometry, due to the combined effects of geometric complexity, mesh conformity requirements, and stability limitations.

2.2. Segregated approach

To overcome the drawbacks of the block-coupled approach, a segregated solver was developed using OpenFOAM 7 [11]as a more flexible and robust alternative. The employed segregated approach is straightforward to implement and offers greater flexibility by applying iterations at fluid–solid interfaces. The structure of the newly developed segregated solver, as well as the formulation of the coupling interface condition, draws inspiration from OpenFOAM's native `chtMultiRegionFoam` solver and the `turbulentTemperatureCoupledBaffleMixedFvPatchScalarField` boundary condition, both of which are part of the library's core source code. It should be mentioned that in parallel with the present development, a multi-region, multiphase MHD solver in OpenFoam has been developed independently at the University of Rome [12].

During each time step, the interface boundary condition uses values from the previous time step to independently solve the computational domain within each physical region. Consequently, the updated interface potential is computed as

$$\phi_f^{t+\Delta t} = \omega\cdot\phi_{S,\mathrm{C}}^{t} + (1-\omega)\cdot\phi_C^{t+\Delta t}, \tag{9}$$

$$\phi_{S,f}^{t+\Delta t} = \omega\cdot\phi_{S,\mathrm{C}}^{t+\Delta t} + (1-\omega)\cdot\phi_C^{t}, \tag{10}$$

revealing the explicit nature of the segregated algorithm.

The segregated approach requires significantly less memory than full implicit coupling and is generally easier to implement. This offers a major advantage for applications involving complex geometries. By employing Arbitrary Mesh Interface (AMI) interpolation [13], this approach naturally handles non-conformal interfaces, which may arise when using fully automatic meshing tools. Furthermore, the solver relies on the continuously enhanced OpenFOAM - Foundation branch which provides access to advanced numerical tools, including adaptive mesh refinement and the most up-to-date pre- and post- processing capabilities, significantly enhancing the solver's efficiency and versatility for complex fusion applications.

In practice, simulations with the segregated approach often require under-relaxation or the use of the semi-implicit PIMPLE algorithm. In contrast, if feasibly applicable, the block-coupled implicit approach often using a PISO algorithm without outer iterations, can yield a lower overall computational cost for strongly coupled problems.

3. Validation and convergence

For validation of the segregated solver, appropriate benchmark test cases were selected (see Fig. 3). The analytical solution of Hunt flow (H65) [14] under the *thin wall approximation* using a wall conductance parameter c [15, p. 34–46] is commonly used for the verification and validation of liquid metal MHD codes, since the numerical prediction of the high velocity jets in thin boundary layers is considered a challenging task as $Ha \gg 1$ [16]. However, Hunt flow fails to adequately characterize the flow for applications involving *thick conducting walls* as present in fusion blankets. Therefore, as validation *Case I*, an exact analytical solution by Sloan and Smith (SS66) [17] for MHD flow in ducts with thick conducting Hartmann walls, perpendicular to the applied magnetic field, is used. The latter reference shows that for

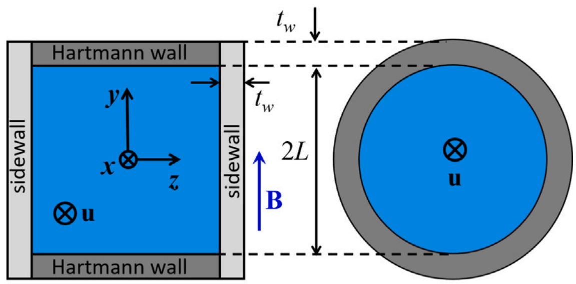

Fig. 3. Sketch of validation cases. *Case I*: MHD flow in a duct with thick electrically conductive Hartmann walls and insulating side walls [17]. *Case II:* rectangular duct flow and *Case III* circular pipe with all conducting walls.

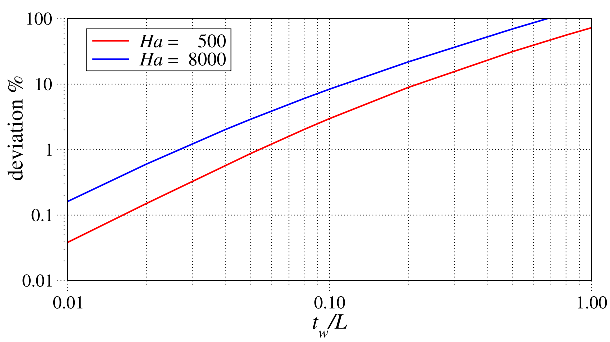

Fig. 4. Relative deviation between pressure gradients obtained for MHD flows in ducts with walls of finite thickness [17] and Hunt's thin-wall solution [14].

Table 2
Case I: Grid convergence study showing relative numerical errors for pressure gradient, maximum velocity, and GCI for $Ha = 500$, t_w/L=0.01, $\sigma_S/\sigma = 1$.

$n_y \times n_z$	K	u_{max}/u_0	GCI
100 × 100	3.34%	2.31%	
200 × 200	1.10%	0.75%	1.70%
300 × 300	0.52%	0.31%	1.22%
400 × 400	0.30%	0.17%	0.75%
600 × 600	0.12%	0.04%	0.37%
800 × 800	0.02%	0.02%	0.32%

Table 3
Case I: Relative numerical errors for pressure gradient and maximum velocity with mesh size 600 × 600, for different Hartmann numbers, t_w/L=0.01, $\sigma_S/\sigma = 1$.

Ha	K	u_{max}/u_0
500	0.12%	0.04%
2500	0.33%	0.27%
5000	0.36%	0.18%
10000	0.24%	0.34%

Table 4
Case II: MHD flow in square duct resolved with 600 × 600 cells with $t_w/L = 0.3$ for all walls, $\sigma_S/\sigma = 0.5$, $Ha = 500$.

Duct	K	u_{max}/u_0
Segregated	25 074.6	4.42794
Block-coupled	25 075.8	4.4279
Differences	0.005%	0.001%

Table 5
Case III: MHD flow in a circular pipe resolved with 367916 cells with t_w/L=0.1, $\sigma_S/\sigma = 0.02$, $Ha = 5000$.

Pipe	K	u_{max}/u_0
Segregated	53 322.8	1.0286
Block-coupled	53 235.9	1.0249
Differences	0.16%	0.36%

values of the wall thickness ratio $t_w/L > 0.01$, velocity profiles deviate significantly from Hunt's solution that is obtained under the thin wall approximation. Specifically, increasing wall thickness to engineering values leads to underestimation of peak velocities and a corresponding overestimation of mean velocity [18].

To illustrate the shortcoming of Hunt flow for applications with thicker walls, the percent deviation in pressure gradient between H65 and SS66 is shown in Fig. 4, where considerable differences are observed when $t_w/L > 0.01$. For the WCLL TBM, where $t_w/L \approx 0.3$ and $Ha \approx 8000$, validation based on the Hunt solution under the thin wall approximation may be inadequate.

For the validation *Case I*, a grid convergence study was performed by comparing numerical results with the exact analytical solution SS66 and by using the Grid Convergence Index (GCI) methodology [19]. Results summarized in Table 2 show a quite good convergence rate for nondimensional pressure gradient $K = -\frac{\partial p}{\partial x}\frac{L^2}{\rho\nu u_0}$ and normalized maximum velocity u_{max}/u_0. Validation results for Case I at different Hartmann numbers, obtained using a 600 × 600 mesh, are presented in Table 3.

Two additional validation cases, referred to as *Case II* and *Case III*, were considered: a square duct and a circular pipe with electrically conducting thick walls. As no exact analytical solutions exist for these configurations, the segregated solver is validated through direct comparison with results from the rigorously validated block-coupled solver [20,21]. The results summarized in Tables 4 and 5 show good agreement.

In the present comparison, both solvers use the same time step size and the PISO algorithm with two corrector loops. It is worth mentioning that the Poisson equation for the electric potential is solved using the BiCGStab solver with a Cholesky preconditioner. In the following, the influence of the interface mesh size ratio δ_S/δ on the convergence rate is analyzed. A similar influence as for σ_S/σ, discussed after definition of ω in Eq. (3) is expected when varying the interface mesh size ratio δ_S/δ for fixed finite σ_S/σ, although the limiting cases $\omega = 0$ and $\omega = 1$ will never be met.

Fig. 5 illustrates the convergence rate of the nondimensional pressure gradient K for a square duct with varying interface mesh size ratios δ_S/δ, while the wall conductance ratio is kept constant at $c = 0.01$. As indicated by Eq. (3), larger values of δ_S/δ corresponds to a smaller value of ω improving convergence speed. Since the mesh in the solid region must remain sufficiently refined to accurately resolve the physical domain, improved convergence may be achieved by finer fluid grids at interfaces. This is consistent with established MHD mesh resolution criteria requiring at least seven grid points across the Hartmann layers and approximately twenty nodes across the side layers for accurate prediction of velocity distribution and pressure gradient in a duct. The latter requirement must be satisfied also for Hartmann numbers in fusion applications where $Ha \approx 8000$ for a WCLL TBM.

A comparison of the convergence behavior of the segregated and block-coupled solvers for the simulation of *Case I* and different wall conditions (t_w/L, σ_S/σ) is presented in Fig. 6. One observes oscillatory convergence for the block-coupled solver and monotonic convergence for the segregated approach. For the strongly electrically coupled interface, as illustrated in the upper subplot, the segregated solver requires roughly two orders of magnitude more execution time to reach convergence due to its explicit iterative nature. In contrast, for the weakly coupled interface, the computational cost of the segregated solver is almost two orders of magnitude lower.

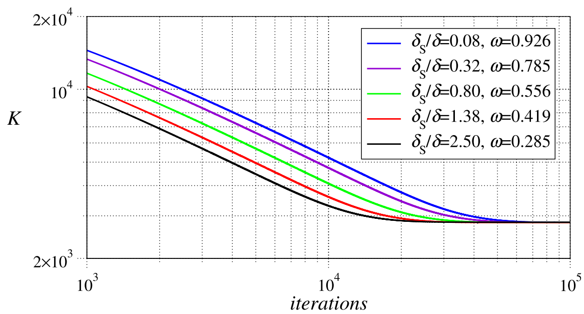

Fig. 5. Convergence rate for nondimensional pressure gradient K of a square duct flow at different interface mesh size ratios δ_S/δ at $Ha = 500$, wall thickness ratio t_w/L=0.01, wall electrical conductivity ratio $\sigma_S/\sigma = 1$.

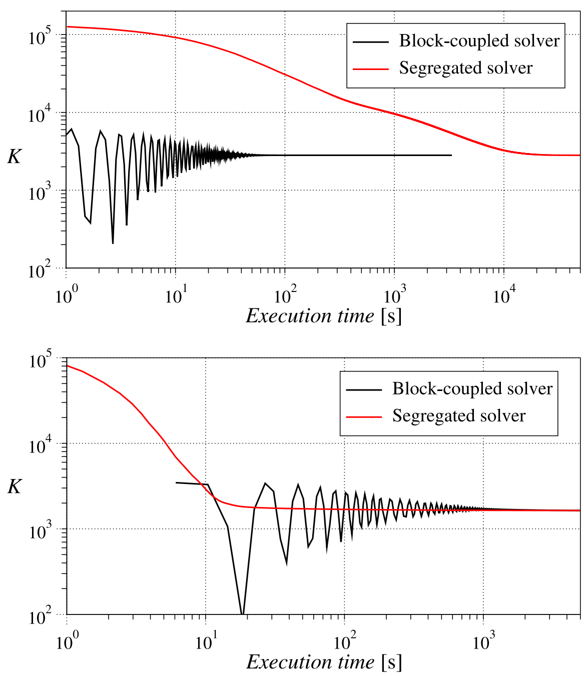

Fig. 6. Comparison of the convergence behavior of the segregated and block-coupled solvers for *Case I* for MHD flow at $Ha = 500$ with same wall conductance parameter $c = 0.01$, but for different wall thickness. Top: $\omega = 0.926$ for t_w/L=0.01, $\sigma_S/\sigma = 1$; bottom: $\omega = 0.943$ for t_w/L=0.5, $\sigma_S/\sigma = 0.02$.

4. Application to simulation for a TBM mock-up

To support the development and potential design revisions of the ITER WCLL TBM, an experimental campaign was conducted at the MEKKA laboratory at KIT, where a representative mock-up was instrumented with electric potential sensors and pressure taps distributed along the liquid metal flow paths [22,23]. The measured data was used to analyze pressure drop relevant to ITER operating conditions [6]. Flow-induced electric potential provides an indirect measure of local flow rates. However, when induced currents shunt through thick electrically conductive walls, the measured surface potential can provide only a qualitative picture. Therefore, numerical simulations play an essential role in order to achieve from measured surface potential data insight into internal details of the flow.

The newly developed and validated segregated solver has been employed to perform numerical simulations of MHD flow in the WCLL TBM mock-up at low magnetic field [24]. In the present study, results have been obtained for stronger imposed magnetic field. While the potential in fluid and wall are coupled at the interface, the outer surface of the wall is electrically insulating. At the entrance a uniform velocity profile is used as a good approximation for fully established MHD pipe flow and at the exit the standard outflow condition is used. This is achieved using an automatically generated, hexahedral-dominated unstructured mesh, without enforcing strict mesh conformity at fluid–solid interfaces. A comprehensive presentation and discussion of all numerical simulation results are beyond the scope of this paper. Instead, a qualitative illustration of the flow paths and the resulting non-uniform flow distribution is provided in Fig. 7.

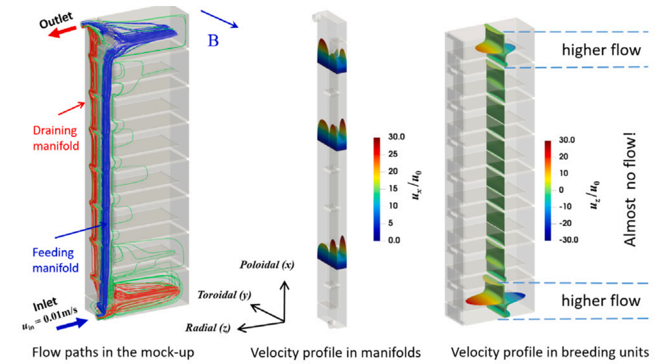

Fig. 7. MHD flow in an entire blanket mock-up without cooling pipes for $Ha = 500$, $N = 6.9 \times 10^4$. Left: flow paths; middle: profiles of poloidal velocity $u_x(y, z)$ in manifolds at three vertical positions; right: profiles of radial velocity $u_z(x, y)$ in the middle plane of BUs.

A large portion of the flow (red streamlines) enters directly BU1, where it moves towards the first wall, reverses direction, and subsequently enters the larger draining manifold, along which it reaches the outlet pipe. Another fraction of the flow (represented by the blue streamlines) proceeds along the feeding manifold up to BU8, through which it enters the draining manifold and ultimately reaches the outlet.

Apart from these main flow paths, only a negligible amount of flow is observed in BUs 2–7. This behavior is further confirmed by velocity profiles in the toroidal-poloidal mid-plane, where significantly higher velocities in BU1 and BU8 are evident. These regions are characterized by jet-like structures along walls parallel to the magnetic field.

The vertical velocity component (Fig. 7 in the middle) indicates that the initially high velocity in the feeding manifold progressively decreases along the poloidal direction, whereas the velocity in the draining manifold increases until both channels reach comparable flow speeds. Beyond this point, the flow rates in the feeding and draining channels remain nearly constant along the poloidal direction until BU8 is reached, through which the remaining fraction of the flow in the feeding manifold exits the system.

The distribution of flow rates between the feeding and draining manifolds as well as through the BUs has been quantified based on the numerical simulations. The results are summarized in Table 6 and illustrated in Fig. 8, where α_f and α_d denote the fraction of the total flow rate in the feeding and draining manifolds, respectively, and $d\alpha$ represents the fraction of flow exchanged between the two manifolds through breeder unit BUi. The results indicate that approximately 48% of the total flow is transferred through BU1, followed by an additional 10% through BU2. The flow in BU3–BU6 is almost negligible, as the flow rates in both manifolds remain nearly constant for $3 \leq i \leq 6$. Towards the downstream end of the module, BU7 transfers about 6.6% of the flow, while BU8 conveys the remaining 32%, thereby confirming the flow patterns observed in the streamline and velocity field analyses. The numerically predicted flow distribution shows good agreement with experimental observations, in which local flow rates were indirectly derived from flow induced electric potential measurements (see e.g. Fig. 11 in [7]).

Table 6
Flow rate fractions of feeding and draining manifolds α_f and α_d along the poloidal direction obtained by numerical simulation with $Ha = 500$. Here, ξ denotes the poloidal position, scaled by the total poloidal length L_{pol} of the mock-up.

Breeding unit		Flow fractions		
i	$\xi = x/L_{pol}$	α_f	α_d	$d\alpha$
	entrance	1.000	0.000	
1	0.0625			0.4757
		0.524	0.476	
2	0.1875			0.0996
		0.424	0.576	
3	0.3125			0.0197
		0.405	0.595	
4	0.4375			0.0047
		0.400	0.600	
5	0.5625			0.0033
		0.396	0.604	
6	0.6875			0.0131
		0.383	0.616	
7	0.8125			0.0664
		0.317	0.683	
8	0.9375			0.3174
	exit	0.000	1.000	$\sum d\alpha = 1$

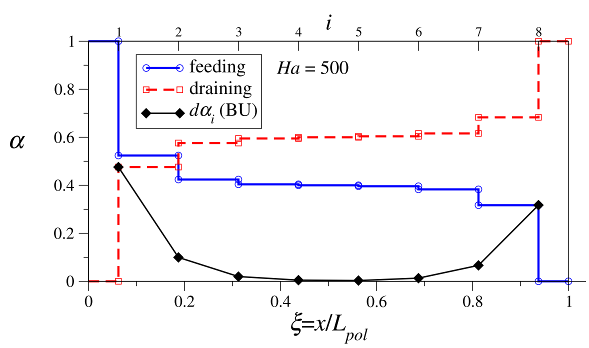

Fig. 8. Distribution of flow rates in feeding (blue) and draining (red) manifolds of a WCLL TBM mock-up along the poloidal coordinate and flow partitioning among BUs (black).

Such non-uniform flow partitioning should be avoided for efficient tritium removal from the TBM. This issue can be mitigated by modifying the geometry of the feeding and draining manifolds, in particular by optimizing the positions of the separating baffle walls along the poloidal direction, as proposed in [25]. It is therefore strongly recommended to update the manifold design and reposition the separating baffle walls to appropriate positions.

5. Conclusions

The present study is motivated by the need for efficient and robust numerical algorithms to predict multi-region MHD flows in liquid metal breeding blankets. Two different approaches for modeling electric coupling were investigated: a block-coupled and a segregated method. The block-coupled approach solves the governing equations simultaneously in all regions, providing strong implicit coupling at interfaces and rapid convergence for simple geometries. However, it requires strict mesh conformity across interfaces, which significantly limits its applicability when automatic meshing tools are used for complex blanket geometries.

To overcome this limitation, a segregated solver was developed and validated. By solving the equations independently in each region with iterative interface conditions, the segregated approach tolerates nonconforming meshes at fluid–solid interfaces. It is therefore well suited for complex geometries, enabling the use of automatic mesh generation techniques thus substantially reducing meshing efforts.

The segregated solver was then applied to simulations of MHD flow in a WCLL TBM mock-up for demonstrating it predictive capability for complex geometries. The results reveal a highly non-uniform liquid metal flow distribution among BUs, with most of the flow passing through BU1 and BU8, and a pronounced asymmetry favoring BU1. A comprehensive presentation of the numerical results and a detailed comparison with experimental data will be reported in a forthcoming dedicated publication.

The comparative assessment of the two numerical approaches highlights their respective strengths and limitations in terms of accuracy, robustness, and computational performance. Based on these findings, the block-coupled approach is recommended for strongly coupled multi-region MHD flows in simple geometries, whereas the segregated approach is better suited for complex geometries when automatic meshing is required.

CRediT authorship contribution statement

B. Lyu: Writing – review & editing, Writing – original draft, Visualization, Validation, Software, Methodology, Investigation, Formal analysis, Data curation, Conceptualization. **L. Bühler:** Writing – review & editing, Supervision, Resources. **C. Mistrangelo:** Writing – review & editing, Supervision, Project administration.

Declaration of competing interest

The authors declare that they have no known competing financial interests or personal relationships that could have appeared to influence the work reported in this paper.

Acknowledgments

This work has been carried out within the framework of the EUROfusion Consortium, funded by the European Union via the Euratom Research and Training Programme (Grant Agreement No 101052200 — EUROfusion). Views and opinions expressed are however those of the author(s) only and do not necessarily reflect those of the European Union or the European Commission. Neither the European Union nor the European Commission can be held responsible for them.

Data availability

Data will be made available on request.

References

[1] J. Aubert, G. Aiello, D. Alonso, T. Batal, R. Boullon, S. Burles, B. Cantone, F. Cismondi, A. Del Nevo, L. Maqueda, A. Morin, E. Rodríguez, F. Rueda, M. Soldaini, J. Vallory, Design and preliminary analyses of the new Water Cooled Lithium Lead TBM for ITER, Fusion Eng. Des. 160 (2020) 111921, http://dx.doi.org/10.1016/j.fusengdes.2020.111921.

[2] C. Koehly, L. Bühler, C. Courtessole, Design of a scaled mock-up of the WCLL TBM for MHD experiments in liquid metal manifolds and breeder units, Fusion Eng. Des. 192 (2023) 113753, http://dx.doi.org/10.1016/j.fusengdes.2023.113753.

[3] H. Madarame, K. Taghavi, M.S. Tillack, The influence of leakage currents on MHD pressure drop, Fusion Technol. 8 (1985) 264–269, http://dx.doi.org/10.13182/FST85-A40055.

[4] K.A. McCarthy, M.A. Abdou, Analysis of liquid metal MHD flow in multiple adjacent ducts using an iterative method to solve the core flow equations, Fusion Eng. Des. 13 (1991) 363–380, http://dx.doi.org/10.1016/0920-3796(91)90092-5.

[5] R. Stieglitz, S. Molokov, Experimental study of magnetohydrodynamic flows in electrically coupled bends, J. Fluid Mech. 343 (1997) 1–28, http://dx.doi.org/10.1017/S0022112097005788.

[6] C. Courtessole, H.-J. Brinkmann, L. Bühler, J. Roth, Characterization of MHD pressure losses in a mock-up of the WCLL test blanket module, Fusion Eng. Des. 219 (2025) 115216, http://dx.doi.org/10.1016/j.fusengdes.2025.115216.

[7] L. Bühler, C. Courtessole, B. Lyu, C. Mistrangelo, Electric potential on a WCLL TBM mock-up in MHD experiments as indication for flow distribution in breeder units, Fusion Eng. Des. 212 (2025) 114846, http://dx.doi.org/10.1016/j.fusengdes.2025.114846.

[8] C. Mistrangelo, L. Bühler, Development of a numerical tool to simulate magneto-hydrodynamic interactions of liquid metals with strong applied magnetic fields, in: Fusion Science and Technology, Fusion Sci. Technol. 60 (2) (2011) 798–803, http://dx.doi.org/10.13182/FST11-A12483.

[9] FOAM-extend, 2025, URL https://sourceforge.net/projects/foam-extend/. (Accessed 08 December 2025).

[10] H. Jasak, OpenFOAM: Open source CFD in research and industry, Int. J. Nav. Archit. Ocean. Eng. 1 (2) (2009) 89–94, http://dx.doi.org/10.2478/IJNAOE-2013-0011.

[11] OpenFOAM-Foundation, Openfoam 7, 2020, URL https://openfoam.org/version/7/.

[12] S. Siriano, L. Melchiorri, S. Pignatiello, A. Tassone, A multi-region and a multiphase MHD OpenFOAM solver for fusion reactor analysis, Fusion Eng. Des. 200 (2024) 114216, http://dx.doi.org/10.1016/j.fusengdes.2024.114216.

[13] P. Farrell, J. Maddison, Conservative interpolation between volume meshes by local Galerkin projection, Comput. Methods Appl. Mech. Engrg. 200 (1) (2011) 89–100, http://dx.doi.org/10.1016/j.cma.2010.07.015, URL https://www.sciencedirect.com/science/article/pii/S0045782510002276.

[14] J.C.R. Hunt, Magnetohydrodynamic flow in rectangular ducts, J. Fluid Mech. 21 (1965) 577–590, http://dx.doi.org/10.1017/S0022112065000344.

[15] U. Müller, L. Bühler, Magnetofluiddynamics in channels and containers, Springer, Wien, New York, 2001, http://dx.doi.org/10.1007/978-3-662-04405-6, ISBN 3-540-41253-0.

[16] S. Smolentsev, S. Badia, R. Bhattacharyay, L. Bühler, L. Chen, Q. Huang, H.-G. Jin, D. Krasnov, D.-W. Lee, E. Mas de les Valls, C. Mistrangelo, R. Munipalli, M.-J. Ni, D. Pashkevich, A. Patel, G. Pulugundla, P. Satyamurthy, A. Snegirev, V. Sviridov, P. Swain, T. Zhou, O. Zikanov, An approach to verification and validation of MHD codes for fusion applications, Fusion Eng. Des. 100 (2015) 65–72, http://dx.doi.org/10.1016/j.fusengdes.2014.04.049.

[17] D.M. Sloan, P. Smith, Magnetohydrodynamic flow in a rectangular pipe between conducting plates, Z. Angew. Math. Mech. 46 (1966) 439–443.

[18] M.J. Bluck, M.J. Wolfendale, An analytical solution to electromagnetically coupled duct flow in MHD, J. Fluid Mech. 771 (2015) 595–623, http://dx.doi.org/10.1017/jfm.2015.202.

[19] P.J. Roache, Perspective: A method for uniform reporting of grid refinement studies, J. Fluids Eng.-Trans. Asme 116 (3) (1994) 405–413, http://dx.doi.org/10.1115/1.2910291.

[20] C. Mistrangelo, L. Bühler, Determination of multichannel MHD velocity profiles from wall-potential measurements and numerical simulations, Fusion Eng. Des. 130 (2018) 137–141, http://dx.doi.org/10.1016/j.fusengdes.2018.03.041.

[21] V. Klüber, Three-Dimensional Magnetohydrodynamic Phenomena in Circular Pipe Flow (Ph.D. thesis), Karlsruhe Institute of Technology, 2023, http://dx.doi.org/10.5445/IR/1000156159.

[22] L. Bühler, H.-J. Brinkmann, C. Courtessole, V. Klüber, C. Koehly, B. Lyu, C. Mistrangelo, J. Roth, Liquid metal MHD research at KIT: fundamental phenomena and flows in complex blanket geometries, Fusion Eng. Des. 200 (2024) 114195, http://dx.doi.org/10.1016/j.fusengdes.2024.114195.

[23] C. Courtessole, H.-J. Brinkmann, L. Bühler, J. Roth, Experimental investigation of MHD flows in a WCLL TBM mock-up, Fusion Eng. Des. 202 (2024) 114306, http://dx.doi.org/10.1016/j.fusengdes.2024.114306.

[24] C. Mistrangelo, L. Bühler, V. Klüber, Towards the simulation of MHD flow in an entire WCLL blanket mock-up, Fusion Eng. Des. 193 (2023) 113752, http://dx.doi.org/10.1016/j.fusengdes.2023.113752.

[25] L. Bühler, C. Mistrangelo, Geometric optimization of electrically coupled liquid metal manifolds for WCLL blankets, IEEE Trans. Plasma Sci. 202 (2024) 114306, http://dx.doi.org/10.1109/TPS.2024.3362689.